

UC Berkeley

UC Berkeley Previously Published Works

Title

Assessment of Adsorbate π -Backbonding in Copper(I) Metal–Organic Frameworks via Multinuclear NMR Spectroscopy and Density Functional Theory Calculations

Permalink

<https://escholarship.org/uc/item/59v2738m>

Journal

The Journal of Physical Chemistry C, 127(15)

ISSN

1932-7447

Authors

Funke, Lena M

Chakraborty, Romit

Carsch, Kurtis M

et al.

Publication Date

2023-04-20

DOI

10.1021/acs.jpcc.3c00462

Copyright Information

This work is made available under the terms of a Creative Commons Attribution License, available at <https://creativecommons.org/licenses/by/4.0/>

Peer reviewed

Assessment of Adsorbate π -Backbonding in Copper(I) Metal–Organic Frameworks via Multinuclear NMR Spectroscopy and Density Functional Theory Calculations

Lena M. Funke, Romit Chakraborty, Kurtis M. Carsch, Martin Head-Gordon, Jeffrey R. Long, and Jeffrey A. Reimer*



Cite This: *J. Phys. Chem. C* 2023, 127, 7513–7519



Read Online

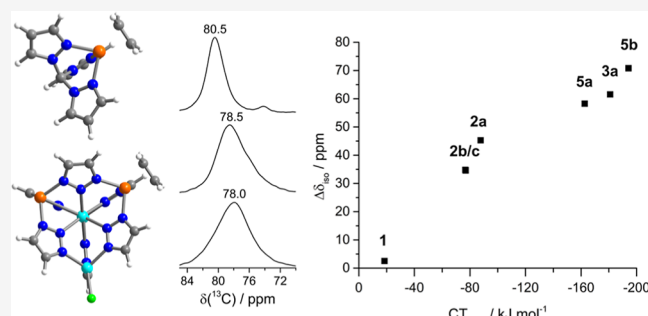
ACCESS |

Metrics & More

Article Recommendations

Supporting Information

ABSTRACT: We assess the binding of C_2H_4 to the coordinately unsaturated copper(I) sites of the metal–organic frameworks Cu(I)-ZrTpmC* and Cu(I)-MFU-4l via ^{13}C solid-state nuclear magnetic resonance spectroscopy, density functional theory (DFT), and natural localized molecular orbital analysis. Using these methods, forward-donation and back-donation contributions between C_2H_4 and the exposed Cu(I) are delineated, and high binding enthalpies are contextualized as a function of electronic changes upon site modification and adsorption. With the infrastructure for DFT and solid-state ^{13}C NMR becoming more routine for scientists, we envision that these results will support the study of exposed electron-rich metal sites in a variety of chemical applications.



INTRODUCTION

For applications such as gas separations, heterogeneous catalysis, and sensing, porous adsorbents offer an energy-efficient alternative to established technologies. In particular, metal–organic frameworks (MOFs) bearing coordinatively unsaturated metal sites can bind gas molecules with selectivities 1 or 2 orders of magnitude larger than traditional adsorbent materials that possess non-specific physisorption interactions. Through judicious choice of the metal ion and linker, one can tailor, for example, strong selective gas binding under a plethora of conditions extending into industrial gas separations, catalysis, and gas storage.¹ Unsaturated metal sites characteristic of some adsorbents—including those in MOFs and zeolites—are electronically Lewis acidic in nature with minimal π -backbonding capabilities. In contrast, π -basic metal sites afford the possibility of strongly adsorbing many substrates. Lewis π -basic sites in MOFs are less common and act either by accepting electrons in free orbitals or donating electrons into adsorbate accessible π^* orbitals, which are referred to as back bonding and forward donation, respectively.

An exemplary MOF hosting Lewis acid sites is Cu(I)-MFU-4l ($Zn_5Cl_4(\text{btdd})_3$; btdd²⁻ = bis[1,2,3-triazolato-[4',5'-i][4',5'-i]]dibenzo[1,4]-dioxin), which was reported in 2014 and features coordinatively unsaturated Cu(I) metal sites that adsorb π -acidic H_2 , O_2 , N_2 , and C_2H_4 .² In 2018, the MOF Cu(I)-ZrTpmC* [Tpm* = tris(3,5-dimethylpyrazolyl)-methane] was reported and observed to catalyze cyclopropanation reactions akin to those promoted by analogous

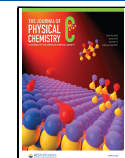
molecular complexes.³ While theoretical approaches have improved to better understand adsorbent–adsorbate interactions involving forward and back donation at Lewis π -basic sites in MOFs,^{4,5} experimental proof-of-impact of synthetic MOF manipulations according to those models is underdeveloped. Open questions include (1) the direction and intensity of charge transfer (CT) and (2) the influence of the chemical environment of the open metal site on the adsorbent–adsorbate interaction. Recently, Cu L-edge near-edge X-ray absorption fine structure measurements performed on Cu(I)-MFU-4l suggest that the energies of the X-ray transitions correlate with the energy levels of the isolated small-molecule adsorbates. The transition intensities were also found to be proportional to the binding energies of the guest molecules within Cu(I)-MFU-4l.⁶

To further understand the effects of guest binding on the structure, dynamics, and electron density distribution, we employ ^{13}C and 1H NMR spectroscopy measurements of ethylene adsorbed within two MOFs with different Cu(I) metal sites and conduct DFT and natural localized molecular

Received: January 23, 2023

Revised: March 25, 2023

Published: April 10, 2023



orbital (NLMO) analyses to better understand the NMR spectra. These analyses are further informed by computational simulations for other ethylene–metal complexes.

The overall nuclear-spin Hamilton operator for a solid is typically expressed as a sum of Hamilton operators,⁷ yet herein we focus on just one of those Hamiltonians, chemical shielding, and in particular the differing chemical shielding between free and adsorbed ethylene. In our study, diamagnetic and paramagnetic effects contribute to the chemical shift and have the potential to impact the characteristic features of the ¹³C NMR spectrum of ethylene adsorbed on different substrates (for a general description of chemical shift, see the Supporting Information).

The effective magnetic field B_{eff} at the site of the nucleus can be described in terms of the sum of the external and the induced magnetic fields $B_{\text{eff}} = B_0 + B_{\text{ind}}$. The induced field is described by the magnetic shielding anisotropy (CSA) tensor $\vec{\sigma}$ interacting with B_0

$$B_{\text{ind}} = \vec{\sigma} B_0 \quad (1)$$

with

$$\vec{\sigma} = \begin{pmatrix} \sigma_{11} & 0 & 0 \\ 0 & \sigma_{22} & 0 \\ 0 & 0 & \sigma_{33} \end{pmatrix} \quad (2)$$

The matrix elements σ_{xx} , σ_{yy} , and σ_{zz} describe the strength of magnetic shielding along three directions in space. The CSA tensor $\vec{\sigma}$ describes the shielding along the Cartesian directions in a principal axis coordinate system. The historical convention for the definition of the principal axis system⁸ is

$$\delta_{\text{iso}} = -\sigma_{\text{iso}} = -1/3(\delta_{11} + \delta_{22} + \delta_{33}) \quad (3)$$

$$\delta_{ii} = -\sigma_{ii} + \delta_{\text{iso}} \text{(reference)} \quad (4)$$

with δ_{iso} (reference) being the chemical shift of a reference compound.

METHODS

Cu(I)-MFU-4l was synthesized following previously reported procedures.^{2,9} In particular, Cu(I)_{2.2}Zn_{2.8}(Cl/HCOO)_{1.8}(btdd)₃ was prepared following thermolysis at 180 °C with subsequent conversion to Cu(I)_{2.2}Zn_{2.8}(Cl/H)_{1.8}(btdd)₃ upon thermolysis at 230 °C, accompanied by evident off-gassing.³ The compound Cu(I)-ZrTpmpC* was also prepared following previously reported procedures.³ The ethylene isotherm for Cu(I)-MFU-4l at 298 K reveals an initial steep uptake (ca. 1.3 mmol/g below 1 mbar), attributed to ethylene coordination to open Cu(I) sites with approximately 70% of Cu sites occupied for stoichiometries of Cu(I)_{2.2}Zn_{2.8}(Cl/H)_{1.8}(btdd)₃(η^2 -C₂H₄)_{1.54} and Cu(I)_{2.2}Zn_{2.8}(Cl/HCOO)_{1.8}(btdd)₃(η^2 -C₂H₄)_{1.54}.⁶ The discrepancy between the calculated and measured ethylene capacity is partially attributed to spectator Cu(II) sites, which have been spectroscopically observed with X-ray absorption spectroscopy and electron paramagnetic resonance spectroscopy.^{6,10}

Isotopically labeled ¹³CH₂=¹³CH₂ (99 atom % ¹³C) was purchased from Sigma-Aldrich, and propene (1-¹³C 99%) and 1-butene (1-¹³C 99%) were purchased from Cambridge Isotope Laboratories.

For NMR measurements, the fully activated MOF was loaded into a rotor in a home-built gas manifold¹¹ inside the

argon atmosphere of a glovebox and evacuated before dosing with the ¹³C-labeled ethylene at ~1000 mbar. The rotor was closed within the manifold, and the samples transferred to a 11.7 T magnet were spun immediately under continuous N₂ flow and with compressed air at 16.4 T.

The magic angle ($\theta = 54.74^\circ$) was set prior to the experiment using KBr. All NMR experiments were acquired at 11.7 T using Bruker 4 mm MAS probes and at 16.4 T using 3.2 mm MAS probes. All ¹³C MAS NMR spectra were acquired using the ¹³C{¹H} cross-polarization experiment at room temperature without temperature control if not stated otherwise.

The ¹³C{¹H} MAS NMR spectra at 16.4 T were recorded with 2 ms contact time, $\tau_p({^1\text{H}}) = 4.0 \mu\text{s}$ at $\nu_r = 3 \text{ kHz}$ with SPINAL64 ¹H decoupling at $\nu_{rf} = 63 \text{ kHz}$ ¹H radio-frequency field-strength. The ¹³C{¹H} heteronuclear correlation (HET-COR) NMR spectra were recorded with 100 μs contact time, $\tau_p({^1\text{H}}) = 4.5 \mu\text{s}$ at $\nu_r = 10 \text{ kHz}$ with TPPM decoupling ($\nu_{rf} = 63 \text{ kHz}$).

The ¹³C{¹H} MAS NMR spectra at 11.7 T were recorded with 2 ms contact time, $\tau_p({^1\text{H}}) = 5.0 \mu\text{s}$ at $\nu_r = 3 \text{ kHz}$ with two-pulse phase-modulation (TPPM) ¹H decoupling ($\nu_{rf} = 33\text{--}54 \text{ kHz}$). Contact times of 200 μs and spinning speeds $\nu_r = 2$, 2.5, 5, and 10 kHz were tested as well. The variable-temperature ¹³C{¹H} MAS NMR spectra were recorded at 11.7 T with $\tau_p({^1\text{H}}) = 3.9 \mu\text{s}$ at $\nu_r = 3 \text{ kHz}$ with TPPM ¹H decoupling ($\nu_{rf} = 64 \text{ kHz}$). The temperature was calibrated based on the chemical shift $\delta(^{79}\text{Br})$ of KBr at $\nu_r = 5 \text{ kHz}$. ¹H NMR spectra were recorded using a 90° pulse sequence at $\nu_r = 3$ and 10 kHz spinning speed with $\tau_p({^1\text{H}}) = 5.0 \mu\text{s}$ at a recycle delay of 2 s; ¹³C and ¹H chemical shifts were referenced using adamantane to 38.5 ppm (tertiary carbon, left-hand resonance) and 1.8 ppm.

RESULTS AND DISCUSSION

Motivated by experimental observations and chemical intuition that the degree of backbonding between a metal site and adsorbent may influence NMR chemical shifts, we first formulated a DFT protocol to probe the magnitude of backbonding for C₂H₄ in various chemical environments using state-of-the art energy decomposition analysis (EDA).^{4,5,12–14} Similar EDA techniques have been used recently to delineate forward- and back-donating contributions for H₂ binding to Cu(I) in MFU-4l and to a V(II) center in a different MOF.^{9,15,16} Here, we calculate the quantitative contributions of $\sigma(\text{C}=\text{C})$, $\pi(\text{C}=\text{C})$, and $\sigma(\text{C}-\text{H})$ to σ_{11} , σ_{22} , σ_{33} , and δ_{iso} in six metal complexes and three molecules: [Ag(η^2 -C₂H₄)]⁺ (1), Cu(I)-MFU-4l(η^2 -C₂H₄) (2a), Cu(I)-MFU-4l(η^2 -C₃H₆) (2b), Cu(I)-MFU-4l(η^2 -1-C₄H₈) (2c), [Pt(II)Cl₃(η^2 -C₂H₄)]⁻ (3a), [HB(3-(CF₃)₅-(Ph)Pz)₃]Au(I)(η^2 -C₂H₄) (5a), [MeB(Pz)₃]⁻Au(I)(η^2 -C₂H₄) (5b), C₂H₄, C₃H₆, and 1-C₄H₈. The occupied orbitals contribute to σ_{ii} according to the energy difference with the unoccupied orbital of proper symmetry, i.e., when the products of irreducible representation of ψ_{occ} , ψ_{unocc} , and σ_{ii} are non-zero. Tables S1–S3 summarize all values for ethylene, propylene, and 1-butylene, respectively. The main contribution to σ_{11} comes from the $\sigma(\text{C}=\text{C})$ bond, and σ_{11} decreases with the rise of the $\pi^*(\text{C}=\text{C})$ energy level, thereby reflecting backdonation. For Cu(I) and Pt(II), 81 and 82% of the changes can be attributed to these effects, demonstrating how back bonding strength is reflected in σ_{11} . The tensor component σ_{33} is unchanged from the gas phase molecules upon binding to the metal centers in Cu(I)-MFU-4l, consistent

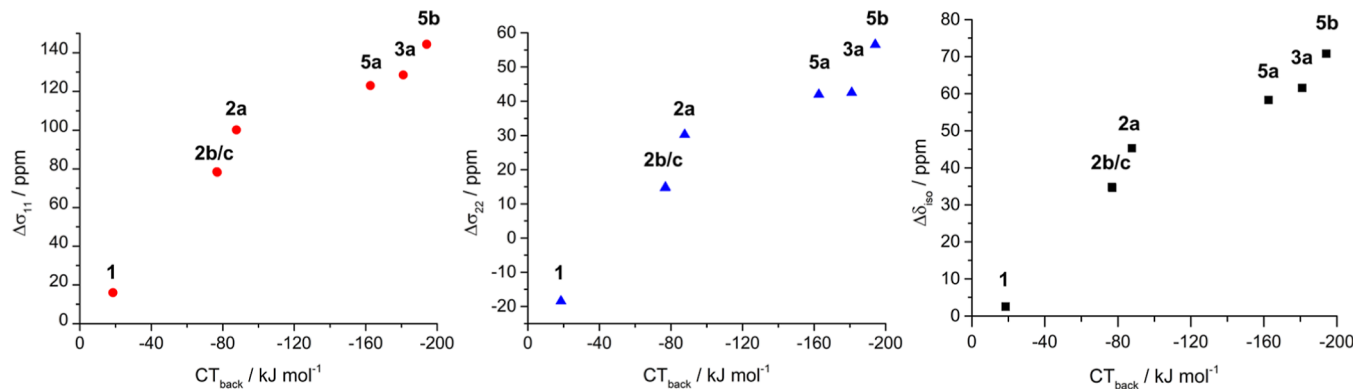


Figure 1. Calculated ^{13}C NMR parameters $\Delta\sigma_{11} = \sigma_{11}(\text{complex}) - \sigma_{11}(\text{molecule})$ (left, red dots), $\Delta\sigma_{22} = \sigma_{22}(\text{complex}) - \sigma_{22}(\text{molecule})$ (center, blue triangles), and $\delta_{\text{iso}} = \delta_{\text{iso}}(\text{molecule}) - \delta_{\text{iso}}(\text{complex})$ (right, black squares) plotted against energy lowering on CT related to π -backbonding (CT_{back}) for $[\text{Ag}(\eta^2\text{-C}_2\text{H}_4)]^+(\mathbf{1})$, $\text{Cu}(\text{I})\text{-MFU-4l}(\eta^2\text{-C}_2\text{H}_4)$ ($\mathbf{2a}$), $\text{Cu}(\text{I})\text{-MFU-4l}(\eta^2\text{-C}_3\text{H}_6)$ ($\mathbf{2b}$), $\text{Cu}(\text{I})\text{-MFU-4l}(\eta^2\text{-1-C}_4\text{H}_8)$ ($\mathbf{2c}$), $[\text{Pt}(\text{II})\text{Cl}_3(\eta^2\text{-C}_2\text{H}_4)]^-(\mathbf{3a})$, $[\text{HB}(3\text{-CF}_3,5\text{-Ph})\text{Pz}]_3\text{Au}(\text{I})(\eta^2\text{-C}_2\text{H}_4)$ ($\mathbf{5a}$), and $[\text{MeB}(\text{Pz})_3]\text{Au}(\text{I})(\eta^2\text{-C}_2\text{H}_4)$ ($\mathbf{5b}$). Experimental data for δ_{ii} have been published for C_2H_4 ,^{17,18} and ($\mathbf{3a}$)^{17,19,20} and computational data for δ_{ii} for C_2H_4 , ($\mathbf{1}$), and ($\mathbf{3a}$).²²

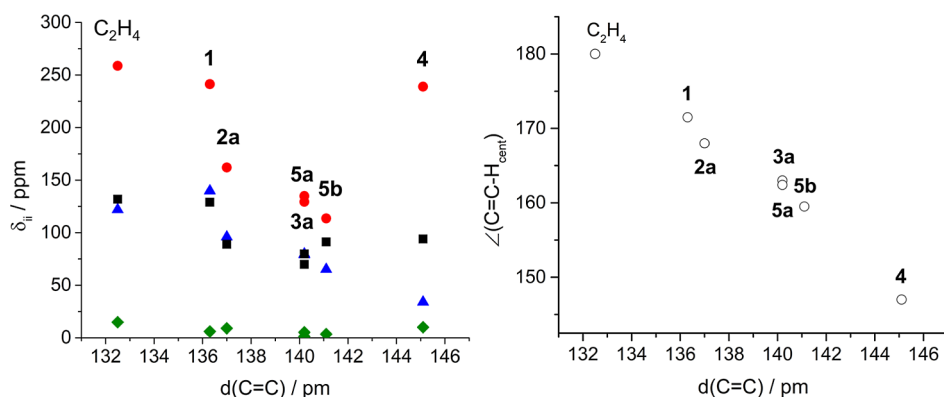


Figure 2. (Left) Computed ^{13}C chemical shifts δ_{11} (red dots), δ_{22} (blue triangles), δ_{33} (green diamonds), and δ_{iso} (black squares) for $[\text{Ag}(\text{I})(\eta^2\text{-C}_2\text{H}_4)]^+$ ($\mathbf{1}$), $\text{Cu}(\text{I})\text{-MFU-4l}(\eta^2\text{-C}_2\text{H}_4)$ ($\mathbf{2a}$), $[\text{Pt}(\text{II})\text{Cl}_3(\eta^2\text{-C}_2\text{H}_4)]^-(\mathbf{3a})$, $\text{Cp}^*\text{Ti}(\text{II})(\eta^2\text{-C}_2\text{H}_4)$ ($\mathbf{4}$), $[\text{HB}(3\text{-CF}_3,5\text{-Ph})\text{Pz}]_3\text{Au}(\text{I})(\eta^2\text{-C}_2\text{H}_4)$ ($\mathbf{5a}$), and $[\text{MeB}(\text{Pz})_3]\text{Au}(\text{I})(\eta^2\text{-C}_2\text{H}_4)$ ($\mathbf{5b}$) according to CSA tensor calculations. (Right) Computed $\text{C}=\text{C}$ distance and $\angle(\text{C}=\text{C}-\text{H}_{\text{cent}})$ angle in C_2H_4 uncoordinated and coordinated to metal centers for the same structures. Experimental data for δ_{ii} have been published for C_2H_4 ,¹⁷ ($\mathbf{1}$),¹⁸ ($\mathbf{3a}$),^{17,19,20} and ($\mathbf{4}$).²¹ Computational data (left, right) for C_2H_4 , ($\mathbf{1}$), ($\mathbf{3a}$), and ($\mathbf{4}$) match well with ref 22.

with experimental observations (vide infra). This absence of change is expected since a combination of the σ_{33} B_{1g} symmetry and a large energy gap between the two perpendicular orbitals $E(\sigma(\text{C}=\text{C})) - E(\sigma(\text{C}-\text{H}))$ leads to small shielding of ethylene, propylene, and butylene along the z -direction that is not expected to change upon binding. In other words, σ_{11} , σ_{22} , and δ_{iso} are related by $-\sigma_{11} - \sigma_{22} = 3\delta_{\text{iso}} + \sigma_{33} \approx 3\delta_{\text{iso}} + 10 \text{ ppm}$.

To further assess the π -backbonding contribution to the NMR chemical shift tensors, we calculated the energy lowering in kJ/mol on CT due to backbonding as distinct from overall CT for different diamagnetic metal centers. We found an increase in the normalized NMR parameters σ_{22} , σ_{11} , and δ_{iso} with an increase in CT related to backbonding (CT_{back}). Figure 1 shows the changes in these parameters after subtracting the values of the adsorbed alkylene, respectively. This analysis suggests that the experimental values of σ_{22} , σ_{11} , and δ_{iso} reflect the extent of CT attributed to π -backbonding. In Figure 2, we examine these calculated parameters in the context of geometric changes in the ethylene molecule within these complexes. The righthand plot shows the $\text{C}=\text{C}$ bond distance increasing linearly with a decreasing out-of-plane angle $\angle(\text{C}=\text{C}-\text{H}_{\text{cent}})$ for metal complexes (the angle between the center of the two H on each side of the molecule in

relation to the $\text{C}=\text{C}$ bond). While $\text{C}=\text{C}$ distance information can be derived via IR spectroscopy, Figure 2 shows that the NMR parameters σ_{iso} , σ_{11} , and σ_{22} are nonlinear with geometric changes and that DFT and NLMO calculations may be paired to give a more detailed description of geometric changes that occur in ethylene upon binding.

We measured ^{13}C solid-state NMR spectra of three MOFs with coordinatively unsaturated $\text{Cu}(\text{I})$ sites (Figure 3). Upon dosing with ethylene, we measured a static ^{13}C NMR spectrum for coordinated $^{13}\text{C}_2\text{H}_4$ in $\text{Cu}(\text{I})\text{-MFU-4l}(\eta^2\text{-C}_2\text{H}_4)$ and $\text{Cu}(\text{I})\text{-ZrTpmC}^*(\eta^2\text{-C}_2\text{H}_4)$. Analysis of the static NMR line shape is experimentally the most reliable way to extract δ_{ii} ($i = 1, 2, 3$). Alternatively, we turned to ^{13}C MAS NMR and compared our experimental spectra with our DFT calculated (vide supra) δ_{iso} , δ_{11} , and δ_{22} .

Experimentally, we find different ^{13}C isotropic chemical shifts for the frameworks $\text{Cu}(\text{I})\text{-ZrTpmC}^*(\eta^2\text{-C}_2\text{H}_4)$ and $\text{Cu}(\text{I})\text{-MFU-4l}(\eta^2\text{-C}_2\text{H}_4)$, as well as for the two $\text{Cu}(\text{I})\text{-MFU-4l}(\eta^2\text{-C}_2\text{H}_4)$ variants with the Zn site coordinated to a mixture of $\text{Cl}^-/\text{HCOO}^-$ or a mixture of Cl^-/H^- (for static ^{13}C NMR spectra, see Figure S5). Briefly, $\text{Cu}(\text{I})\text{-MFU-4l}$ was prepared following the literature procedures,^{2,9} with $\sim 85\%$ of the peripheral chloride anions exchanged for formate anions, as quantified through ^1H NMR spectroscopy following dissolu-

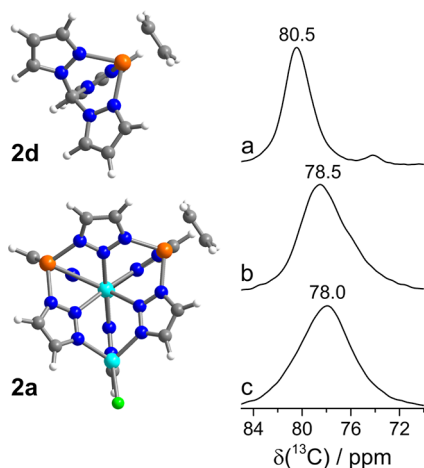


Figure 3. (Left) Complexes of Cu(I)-ZrTpmC*($\eta^2\text{-C}_2\text{H}_4$) (**2d**) and Cu(I)-MFU-4l($\eta^2\text{-C}_2\text{H}_4$) (**2a**) used for calculations in this study. (Right) ^{13}C MAS NMR spectra of (a) $[\text{Cu(I)}\text{-ZrTpmC}^*(\eta^2\text{-C}_2\text{H}_4)]$ (**2d**), (b) $\text{Cu(I)}_{22}\text{Zn}_{28}(\text{Cl}/\text{HCOO})_{18}(\text{btdd})_3(\eta^2\text{-C}_2\text{H}_4)$ (**2e**), and (c) $\text{Cu(I)}_{22}\text{Zn}_{28}(\text{Cl}/\text{H})_{18}(\text{btdd})_3(\eta^2\text{-C}_2\text{H}_4)$ (**2f**). Cyan, orange, green, blue, gray, and white spheres represent Zn, Cu, Cl, N, C, and H atoms, respectively. Full frequency range ^{13}C MAS NMR spectra are depicted in Figure S4.

tion in $\text{DMSO}-d_6/\text{D}_2\text{SO}_4$. Thermolysis at $180\text{ }^\circ\text{C}$ for 1 h under vacuum afforded a mixture of chloride and formate anions at the Zn sites, whereas further thermolysis at $230\text{ }^\circ\text{C}$ for 3 h afforded zinc-formate decomposition to yield a mixture of chloride and hydride anions at the Zn sites.

We find small differences in $\delta_{\text{iso}}(^{13}\text{C}) = 78.0\text{--}79.0\text{ ppm}$ upon ethylene coordination in Cu(I)-MFU-4l and 80.5 ppm for ethylene coordination in Cu(I)-ZrTpmC*($\eta^2\text{-C}_2\text{H}_4$) (see Table 1). For hydride substituents in $\text{Cu(I)}_{22}\text{Zn}_{28}(\text{Cl}/\text{H})_{18}(\text{btdd})_3(\eta^2\text{-C}_2\text{H}_4)$ (**2f**)

Table 1. Experimental and Calculated ^{13}C NMR Chemical Shifts of $^{13}\text{C}_2\text{H}_4$ in Different Cu(I)-Containing MOFs

δ_{ii} (^{13}C)/ppm	δ_{iso}	δ_{11}	δ_{22}	δ_{33}
Experimental ^a				
Cu(I)-ZrTpmC*($\eta^2\text{-C}_2\text{H}_4$) (2d)	80.5			
$\text{Cu(I)}_{22}\text{Zn}_{28}(\text{Cl}/\text{HCOO})_{18}(\text{btdd})_3(\eta^2\text{-C}_2\text{H}_4)$ (2e)	78.5	113	113	~ 10
$\text{Cu(I)}_{22}\text{Zn}_{28}(\text{Cl}/\text{H})_{18}(\text{btdd})_3(\eta^2\text{-C}_2\text{H}_4)$ (2f)	78.0			
CSA Simulations ^b				
C_2H_4 (molecule, solid-state)	126	253	116	9
$\text{Cu(I)}_2\text{Zn}_3(\text{Cl})(\text{btdd})_3(\eta^2\text{-C}_2\text{H}_4)$ cluster	80	152	85	4

^a Recorded at room temperature; experimental error: $\Delta\delta_{\text{iso}} = \pm 0.1\text{ ppm}$. ^b See the Supporting Information for computational details.

$\text{H})_{1.8}(\text{btdd})_3(\eta^2\text{-C}_2\text{H}_4)$, the ^{13}C shifts are slightly higher with 78.0 ppm (HCOO^- : 78.5 ppm), indicating stronger binding for the electron-donating hydride compared to the bulkier chloride ligand, and with the bidentate formate ligand falling in the intermediary range. This emphasizes the sensitivity of the ^{13}C NMR spectra for detecting small changes in the MOF that can impact the nature of adsorbate binding, for example, showing slightly stronger π -backbonding. The ^{13}C MAS NMR data portend that electron-donating groups coordinated to neighboring Zn(II) sites can measurably increase the binding energy of ethylene to Cu(I). The isotropic chemical shift of $\delta_{\text{iso}}(^{13}\text{C}) = 78\text{ ppm}$ compared to 126 ppm for pure ethylene reflects the electronic changes upon π -backbonding. DFT and NLMO analyses allow us to assign the origin to decreasing $\delta_{ii}(^{13}\text{C})$ ($i = 1, 2$) when $\pi^*(\text{C}=\text{C})$ rises in energy compared to $\sigma(\text{C}=\text{C})$ and $\sigma(\text{C}-\text{H})$, respectively.

To elucidate the response of the guest to confinement at the Cu(I) site, we measured ^{13}C NMR spectra as a function of temperature and magnitude of magnetic field (Figure 4). At both 11.7 and 16.4 T , good fits were obtained with the CSA and ^{13}C - ^{13}C dipole–dipole coupling parameters, as derived from DFT. At lower temperatures (see Figure S2), the spinning side bands observed at low ppm increase in relative intensity, indicating a slight increase in δ_{11} , while the center of the spectrum shifts to larger chemical shifts (i.e., δ_{iso} decreases, see Figure S3). The best fit simulating (c in Figure 4) the experimental data in Figure 4a illustrates that from room temperature down to 255 K (see Figure S2), the line shape of ethylene is best fit with a model that assumes the ethylene molecule rapidly rotates when bound to the metal center and effectively averages σ_{11} and σ_{22} . This is consistent with a small rotation barrier height of 2.0 kJ/mol obtained from DFT simulations (see Figure S1). Thus, via ^{13}C MAS NMR combined with DFT calculations, we find that ethylene is adsorbed at the Cu(I) center while spinning around the C_3 z -axis in Cu(I)-MFU-4l, effectively averaging out anisotropy in the xy plane.

To discern the isotropic ^1H NMR chemical shift of C_2H_4 in Cu(I)-MFU-4l($\eta^2\text{-C}_2\text{H}_4$), we turned to $^{13}\text{C}\{^1\text{H}\}$ HETCOR spectroscopy. This double resonance NMR experiment transfers magnetization from protons (^1H) to adjacent ^{13}C nuclear spins. As dipole–dipole coupling decreases with the third power of the internuclear distance $\propto r(\text{C}-\text{H})^{-3}$, the final 2D spectrum at short contact times ($100\text{ }\mu\text{s}$) features those ^1H in direct proximity of ^{13}C , for example, the protons in $^{13}\text{C}_2\text{H}_4$. Figure 5 (left) shows the linear fit of the $\text{C}=\text{C}$ distance in ethylene as a function of the ^1H chemical shifts of different metal complexes. The distance for Cu(I)-MFU-4l derived from our DFT calculations agrees well with the distance predicted

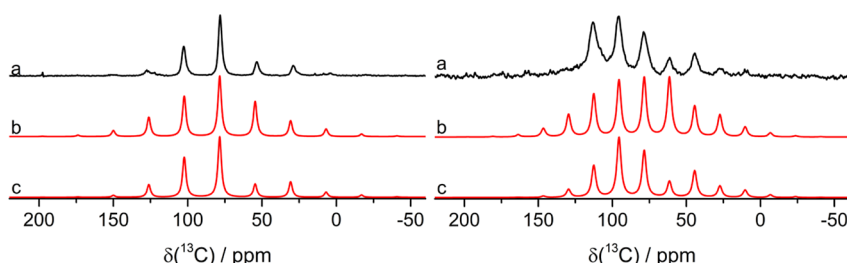


Figure 4. ^{13}C MAS NMR spectra of Cu(I)-MFU-4l($\eta^2\text{-C}_2\text{H}_4$) (**2a**) at (left) 11.7 T and (right) 16.4 T . (a) Experimental; (b,c) simulated two-spin system with a $^{13}\text{C}=^{13}\text{C}$ distance and CSA as simulated for the benzotriazolate-truncated $\text{Cu(I)}_2\text{Zn}_3(\text{Cl})_2(\text{N}_5\text{C}_6\text{H}_4)_6(\eta^2\text{-C}_2\text{H}_4)_2$ with $d(\text{C}=\text{C}) = 137\text{ pm}$: (b) resting and (c) with C_2H_4 spinning around C_3 axis of the Cu(I)-MFU-4l Cu(I) site.

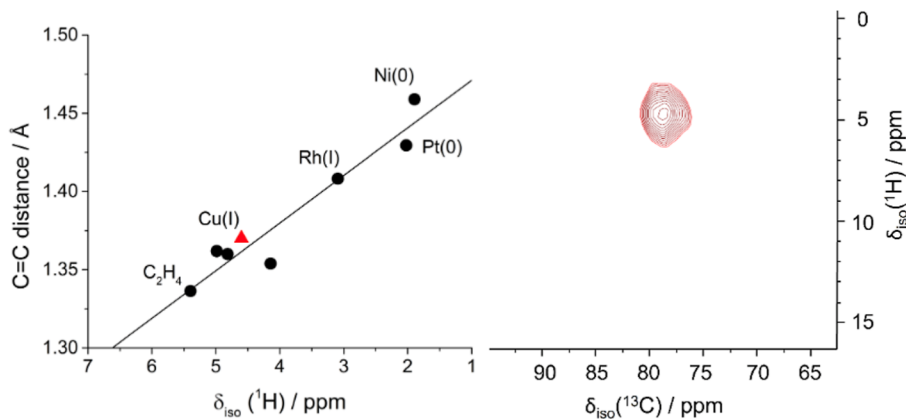


Figure 5. (Left) ^1H NMR isotropic chemical shifts of C_2H_4 in metal complexes²³ and $\text{Cu}(\text{I})\text{-MFU-4l}(\eta^2\text{-C}_2\text{H}_4)$ (**2a**) (red triangle). (Right) $^{13}\text{C}\{^1\text{H}\}$ HETCOR spectrum of $\text{Cu}(\text{I})_{2.2}\text{Zn}_{2.8}(\text{Cl}/\text{H})_{1.8}(\text{btdd})_3(\eta^2\text{-C}_2\text{H}_4)$ (**2f**).

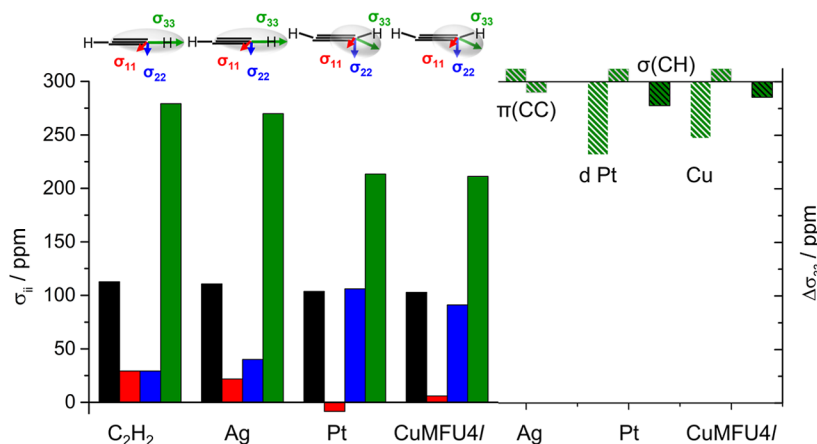


Figure 6. (Left) CSA tensor components in acetylene according to DFT σ_{11} (red), σ_{22} (blue), σ_{33} (green), and σ_{iso} (black); at the top are principal axes relative to the molecular frame. (Right) Orbital contributions attributed to a decline in $\sigma_{33}(\text{C}^{13})$ (green) according to NLMO calculations of $^{13}\text{C}_2\text{H}_2$ in metal complexes: $[\text{Ag}(\text{I})(\eta^2\text{-C}_2\text{H}_2)]^+$ (**1b**), $[\text{Pt}(\text{II})\text{Cl}_3(\eta^2\text{-C}_2\text{H}_2)]^-$ (**3b**), and $\text{Cu}(\text{I})\text{-MFU-4l}(\eta^2\text{-C}_2\text{H}_2)$ (**2g**): $\pi(\text{CC})$ in C_2H_2 (green-yellow striped), d orbital of Pt and s/p orbitals of Cu metal (green-white striped d(Pt) and Cu), and $\pi(\text{CC})$ in C_2H_2 (green-black striped).

by the ^1H NMR shift from the site-resolved $^{13}\text{C}\{^1\text{H}\}$ HETCOR experiment (right). This observation suggests that the isotropic ^1H NMR chemical shift is a good predictor of the geometrical changes in ethylene, specifically the $\text{C}=\text{C}$ distance and the $\angle(\text{C}=\text{C}-\text{H}_{\text{cent}})$ angle. This also applies to the MOF $\text{Cu}(\text{I})\text{-MFU-4l}$.

To measure the contribution of the metal center to forward electron donation, we chose acetylene in lieu of ethylene. Computing the ^{13}C chemical shielding anisotropy tensors of acetylene, we found σ_{33} reflects the metal orbital contribution to forward bonding electron donation.

Figure 6 shows how the orientation of σ_{33} slightly tilts from the $\text{C}\equiv\text{C}$ axis for $[\text{Pt}(\text{II})\text{Cl}_3(\eta^2\text{-C}_2\text{H}_2)]^-$ and $\text{Cu}(\text{I})\text{-MFU-4l}(\eta^2\text{-C}_2\text{H}_2)$. The NLMO analysis (Figure 6, right) highlights the orbital contribution to the paramagnetic component of σ_{33} and the origin of the decrease of σ_{33} upon binding. In $[\text{Ag}(\eta^2\text{-C}_2\text{H}_2)]^+$, σ_{33} stays almost constant compared to C_2H_4 as the two contributions of $\pi(\text{C}\equiv\text{C})$ (see Figure 6, right) cancel each other out. In $[\text{Pt}(\text{II})\text{Cl}_3(\eta^2\text{-C}_2\text{H}_2)]^-$ and the complex of $\text{Cu}(\text{I})\text{-MFU-4l}(\eta^2\text{-C}_2\text{H}_2)$, the metal orbital contributions decrease σ_{33} . This observation suggests that with σ_{33} almost parallel to $\text{C}\equiv\text{C}$, the ^{13}C solid-state NMR spectrum of $^{13}\text{C}_2\text{H}_2$ adsorbed on a metal center should probe the forward donation contribution of the metal center. Our NMR computations show that the ^{13}C -acetylene NMR shifts serve as a probe for

ranking metal centers based on their forward donating contribution.

CONCLUSIONS

Carbon-13 NMR chemical shift simulations predict orbital contributions of the metal base/ π -acid interactions in MOFs. We find that π -backbonding dominates the interaction as discerned from the ^{13}C chemical shielding anisotropy. While the ^{13}C NMR spectrum of ethylene is almost uninfluenced by forward donation— σ_{11} , σ_{22} , and σ_{33} only depend on $E(\sigma(\text{C}=\text{C}))$, $E(\pi^*(\text{C}=\text{C}))$, $E(\sigma(\text{C}-\text{H}))$ —the extent of forward donation can best be evaluated by considering the ^{13}C NMR spectrum of acetylene. The ^1H NMR spectrum of ethylene reflects the overall physical changes upon binding with the isotropic shift, directly correlating with $d(\text{C}=\text{C})$ and $\angle(\text{C}=\text{C}-\text{H}_{\text{cent}})$. In the future, such observations of the electronic structure may help in the design of metal sites with enhanced backbonding interactions in porous materials for gas separation. We envision our approach to be broadly relevant to the study of catalysis and gas adsorption involving alkenes and alkynes in porous framework materials.

ASSOCIATED CONTENT

SI Supporting Information

The Supporting Information is available free of charge at <https://pubs.acs.org/doi/10.1021/acs.jpcc.3c00462>.

Additional remarks on chemical shielding; computational details of NMR parameters; details of DFT calculations on structural refinement, CT, and the C_3 axis rotation of ethylene bound to Cu(I) in MFU-4l; details of fitting the ^{13}C MAS NMR line shape; orbital contributions to chemical shielding anisotropy of ethylene, propylene, and 1-butylene; calculated energy lowering on CT in metal complexes due to forward donation and backbonding; and extended complementary NMR spectroscopic experimentation ([PDF](#))

AUTHOR INFORMATION

Corresponding Author

Jeffrey A. Reimer — Department of Chemical and Biomolecular Engineering, University of California Berkeley, Berkeley, California 94720, United States; Materials Sciences Division, Lawrence Berkeley National Laboratory, Berkeley, California 94720-8099, United States; Email: reimer@berkeley.edu

Authors

Lena M. Funke — Department of Chemistry, University of California Berkeley, Berkeley, California 94720, United States; Department of Chemical and Biomolecular Engineering, University of California Berkeley, Berkeley, California 94720, United States;  orcid.org/0009-0003-7489-9557

Romit Chakraborty — Department of Chemistry, University of California Berkeley, Berkeley, California 94720, United States; Materials Sciences Division, Lawrence Berkeley National Laboratory, Berkeley, California 94720-8099, United States

Kurtis M. Carsch — Department of Chemistry, University of California Berkeley, Berkeley, California 94720, United States;  orcid.org/0000-0003-4432-7518

Martin Head-Gordon — Department of Chemistry, University of California Berkeley, Berkeley, California 94720, United States; Chemical Sciences Division, Lawrence Berkeley National Laboratory, Berkeley, California 94720-8099, United States;  orcid.org/0000-0002-4309-6669

Jeffrey R. Long — Department of Chemistry, University of California Berkeley, Berkeley, California 94720, United States; Department of Chemical and Biomolecular Engineering, University of California Berkeley, Berkeley, California 94720, United States; Materials Sciences Division, Lawrence Berkeley National Laboratory, Berkeley, California 94720-8099, United States;  orcid.org/0000-0002-5324-1321

Complete contact information is available at: <https://pubs.acs.org/doi/10.1021/acs.jpcc.3c00462>

Notes

The authors declare no competing financial interest.

ACKNOWLEDGMENTS

The experimental portions of this research were supported by the U.S. Department of Energy (DOE), Office of Science, Office of Basic Energy Sciences, under award DE-SC0019992.

Computational portions of this research were supported by the Hydrogen Materials—Advanced Research Consortium (HyMARC), established as part of the Energy Materials Network under the U.S. DOE, Office of Energy Efficiency and Renewable Energy, under contract no. DE-AC02-05CH11231. DFT calculations implemented through Gaussian 16 and ADF 2020 were supported by the Molecular Graphics and Computation Facility of the UC Berkeley College of Chemistry that is supported by NIH S10OD023532. We thank Prof. M. Dincă and Dr. C. Sun (MIT) for providing Cu(I)-ZrTpmC*, Dr. Hasan Celik for assistance with NMR VT instrumentation, the Alexander von Humboldt Foundation for a Feodor Lynen Postdoctoral Research Fellowship to L.M.F., and the Arnold and Mabel Beckman Foundation for supporting K.M.C. through an Arnold O. Beckman Postdoctoral Fellowship.

REFERENCES

- (1) Li, J. R.; Kuppler, R. J.; Zhou, H. C. Selective Gas Adsorption and Separation in Metal–Organic Frameworks. *Chem. Soc. Rev.* **2009**, *38*, 1477–1504.
- (2) Denysenko, D.; Grzywa, M.; Jelic, J.; Reuter, K.; Volkmer, D. Scorpionate-Type Coordination in MFU-4l Metal-Organic Frameworks: Small-Molecule Binding and Activation upon the Thermally Activated Formation of Open Metal Sites. *Angew. Chem., Int. Ed.* **2014**, *53*, 5832–5836.
- (3) Sun, C.; Skorupskii, G.; Dou, J.-H.; Wright, A. M.; Dincă, M. Reversible Metalation and Catalysis with a Scorpionate-like Metalloc-Ligand in a Metal–Organic Framework. *J. Am. Chem. Soc.* **2018**, *140*, 17394–17398.
- (4) Khalilullin, R. Z.; Cobar, E. A.; Lochan, R. C.; Bell, A. T.; Head-Gordon, M. Unravelling the Origin of Intermolecular Interactions Using Absolutely Localized Molecular Orbitals. *J. Phys. Chem. A* **2007**, *111*, 8753–8765.
- (5) Loipersberger, M.; Mao, Y.; Head-Gordon, M. Variational Forward-Backward Charge Transfer Analysis Based on Absolutely Localized Molecular Orbitals: Energetics and Molecular Properties. *J. Chem. Theory Comput.* **2020**, *16*, 1073–1089.
- (6) Su, G. M.; Wang, H.; Barnett, B. R.; Long, J. R.; Prendergast, D.; Drisdell, W. S. Backbonding Contributions to Small Molecule Chemisorption in a Metal-Organic Framework with Open Copper(i) Centers. *Chem. Sci.* **2021**, *12*, 2156–2164.
- (7) Duer, M. J. *Introduction to Solid-State NMR Spectroscopy*; Wiley-Blackwell: Oxford, UK, 2004.
- (8) Harris, R. K.; Becker, E. D.; Cabral De Menezes, S. M.; Granger, P.; Hoffman, R. E.; Zilm, K. W. Further Conventions for NMR Shielding and Chemical Shifts (IUPAC Recommendations 2008). *Pure Appl. Chem.* **2008**, *80*, 59–84.
- (9) Barnett, B. R.; Evans, H. A.; Su, G. M.; Jiang, H. Z. H.; Chakraborty, R.; Banyeretse, D.; Hartman, T. J.; Martinez, M. B.; Trump, B. A.; Tarver, J. D.; et al. Observation of an Intermediate to H₂ Binding in a Metal–Organic Framework. *J. Am. Chem. Soc.* **2021**, *143*, 14884–14894.
- (10) Mohamed, M. H.; Yang, Y.; Li, L.; Zhang, S.; Ruffley, J. P.; Jarvi, A. G.; Saxena, S.; Veser, G.; Johnson, J. K.; Rosi, N. L. Designing Open Metal Sites in Metal-Organic Frameworks for Paraffin/Olefin Separations. *J. Am. Chem. Soc.* **2019**, *141*, 13003–13007.
- (11) Forse, A. C.; Milner, P. J.; Lee, J.-H.; Redfearn, H. N.; Oktawiec, J.; Siegelman, R. L.; Martell, J. D.; Dinakar, B.; Zasada, L. B.; Gonzalez, M. I.; et al. Elucidating CO₂ Chemisorption in Diamine-Appended Metal–Organic Frameworks. *J. Am. Chem. Soc.* **2018**, *140*, 18016–18031.
- (12) Horn, P. R.; Mao, Y.; Head-Gordon, M. Defining the Contributions of Permanent Electrostatics, Pauli Repulsion, and Dispersion in Density Functional Theory Calculations of Intermolecular Interaction Energies. *J. Chem. Phys.* **2016**, *144*, 114107.

- (13) Levine, D. S.; Horn, P. R.; Mao, Y.; Head-Gordon, M. Variational Energy Decomposition Analysis of Chemical Bonding. 1. Spin-Pure Analysis of Single Bonds. *J. Chem. Theory Comput.* **2016**, *12*, 4812–4820.
- (14) Khaliullin, R. Z.; Bell, A. T.; Head-Gordon, M. Analysis of Charge Transfer Effects in Molecular Complexes Based on Absolutely Localized Molecular Orbitals. *J. Chem. Phys.* **2008**, *128*, 184112.
- (15) Jaramillo, D. E.; Jiang, H. Z. H.; Evans, H. A.; Chakraborty, R.; Furukawa, H.; Brown, C. M.; Head-Gordon, M.; Long, J. R. Ambient-Temperature Hydrogen Storage via Vanadium(II)-Dihydrogen Complexation in a Metal–Organic Framework. *J. Am. Chem. Soc.* **2021**, *143*, 6248–6256.
- (16) Chakraborty, R.; Carsch, K. M.; Jaramillo, D. E.; Yabuuchi, Y.; Furukawa, H.; Long, J. R.; Head-Gordon, M. Prediction of Multiple Hydrogen Ligation at a Vanadium(II) Site in a Metal–Organic Framework. *J. Phys. Chem. Lett.* **2022**, *13*, 10471–10478.
- (17) Zilm, K. W.; Conlin, R. T.; Grant, D. M.; Michl, J. Low-Temperature Carbon-13 Magnetic Resonance of Solids. 1. Alkenes and Cycloalkenes. *J. Am. Chem. Soc.* **1980**, *102*, 6672–6676.
- (18) Reisinger, A.; Trapp, N.; Knapp, C.; Himmel, D.; Breher, F.; Rüegger, H.; Krossing, I. Silver–Ethene Complexes $[\text{Ag}(\text{H}_2\text{C}_2\text{H}_4)_n][\text{Al}(\text{ORF})_4]$ with $\text{N}=1, 2, 3$ (RF=Fluorine-Substituted Group). *Chem.—Eur. J.* **2009**, *15*, 9505–9520.
- (19) Huang, Y.; Gilson, D. F. R.; Butler, I. S. Carbon-13 Shielding Tensors of Zeise's Salt and Zeise's Dimer. *J. Chem. Soc., Dalton Trans.* **1992**, *19*, 2881–2883.
- (20) Facelli, J. C.; Orendt, A. M.; Beeler, A. J.; Solum, M. S.; Depke, G.; Malsch, K. D.; Downing, J. W.; Murthy, P. S.; Grant, D. M.; Michl, J. Low-Temperature ^{13}C Magnetic Resonance in Solids. 5. Chemical Shielding Anisotropy of the $^{13}\text{CH}_2$ Group. *J. Am. Chem. Soc.* **1985**, *107*, 6749–6754.
- (21) Gordon, C. P.; Shirase, S.; Yamamoto, K.; Andersen, R. A.; Eisenstein, O.; Copéret, C. NMR Chemical Shift Analysis Decodes Olefin Oligo- and Polymerization Activity of D0 Group 4 Metal Complexes. *Proc. Natl. Acad. Sci. U.S.A.* **2018**, *115*, E5867–E5876.
- (22) Gordon, C. P.; Andersen, R. A.; Copéret, C. Metal Olefin Complexes: Revisiting the Dewar–Chatt–Duncanson Model and Deriving Reactivity Patterns from Carbon-13 NMR Chemical Shift. *Helv. Chim. Acta* **2019**, *102*, No. e1900151.
- (23) Suenaga, Y.; Ping Wu, L.; Kuroda-Sowa, T.; Munakata, M.; Maekawa, M. Structure and ^1H NMR Study of Copper(I) Complex with Ethylene and Tetramethylethylenediamine. *Polyhedron* **1997**, *16*, 67–70.

Recommended by ACS

Permanent Porosity in the Room-Temperature Magnet and Magnonic Material V(TCNE)

Jesse G. Park, Jeffrey R. Long, et al.

MARCH 28, 2023

ACS CENTRAL SCIENCE

READ

Kinetics of Guest-Induced Structural Transitions in Metal–Organic-Framework MIL-53(Al)-NH₂ Probed by High-Pressure Nuclear Magnetic Resonance

Jeremias C. Zill, Rustem Valiullin, et al.

MARCH 30, 2023

THE JOURNAL OF PHYSICAL CHEMISTRY LETTERS

READ

Electron Density Analysis of Metal–Metal Bonding in a Ni₄ Cluster Featuring Ferromagnetic Exchange

Sofie Stampe Leiszner, Jacob Overgaard, et al.

DECEMBER 22, 2022

INORGANIC CHEMISTRY

READ

Bonding Nature of “Ionic Carbenes” in [M₃(μ₃-CH₂)]-Containing Compounds: The Covalent Interaction

Yun-Shu Cui, Jun Li, et al.

JULY 25, 2022

INORGANIC CHEMISTRY

READ

Get More Suggestions >